Thesis for the Degree of Master of Science

Development of a dispersion model for two-phase chemical agents considering dry deposition effect

by
Sangcheol Han
Division of Earth Environmental System Science
(Major of Environmental Atmospheric Sciences)
The Graduate school
Pukyong National University

February, 2024

Development of a dispersion model for two-phase chemical agents considering dry deposition effect (건성 침적 효과를 고려한 이상 화학작용제 확산 모델 개발)

Advisor: Prof. Jae-Jin Kim

by
Sangcheol Han

A thesis submitted in partial fulfillment of the requirements
for the degree of

Master of Science

in Division of Earth Environmental System Science
(Major of Environmental Atmospheric Sciences),
the Graduate School,
Pukyong National University

February 2024

Development of a dispersion model for two-phase chemical agents considering dry deposition effect

A dissertation
by
Sangcheol Han

Approved by:

_____

(Chairman) Prof. Wonsik Choi

_____ _____

(Member) Prof. Woosok Moon (Member) Prof. Jae-Jin Kim

February 16, 2024

Contents

List of Figures · ii
Abstract · iv

Ⅰ. Introduction · 1

Ⅱ. Methods · 4
2.1. Numerical model · 4
2.2. Numerical setup · 9

Ⅲ. Results and discussion · · · · · · · · · · · · · · · · · · 13
3.1. Control Experiment · · · · · · · · · · · · · · · · · · · 13
3.2. Effects of the ambient wind speeds · · · · · · · · · · 20
3.3. Effects of the dry deposition · · · · · · · · · · · · · · 30
3.4. Effects of the Evaporation rate · · · · · · · · · · · · 36

Ⅳ. Summary and conclusions · · · · · · · · · · · · · · · · 41

References · 43

Appendix · 52

Acknowledgements · 54

List of Figures

Figure 1. The numerical domain and building configuration used in this study. · · · 12

Figure 2. Wind vectors and contours of the wind speeds normalized by U_{ref} at $y/H = 0$ in CNTL. · · · 15

Figure 3. Streamlines starting at $z/H = 0.16$ and 0.33 around the street canyon. Colors indicate the wind speeds normalized by U_{ref}. · · · 16

Figure 4. Contours of the concentrations of the (a) liquid− and (b) gas−phase chemical agents at $y/H = 0$ in CNTL. · · · 17

Figure 5. When a source is located within the street canyon, contours of the concentrations of the (a) liquid−phase and (b) gas−phase chemical agents at $y/H = 0$ in CNTL. · · · 19

Figure 6. Streamlines and contours of wind speeds normalized by at U_{ref} $z/H = 0.5$ in (a) EU0.5, (b) CNTL, (c) EU20, and (d) EU30. · · · 22

Figure 7. Wind vectors and contours of the wind speeds normalized by U_{ref} at $y/H = 0$. in (a) EU0.5, (b) EU20, and (c) EU30. · · · 23

Figure 8. Contours of liquid−phase chemical agents at $y/H = 0$ in (a) EU05, (b) CNTL, (c) EU20, and (d) EU30. · · · 26

Figure 9. The same as in Fig. 8 except for gas−phase chemical agents. 27

Figure 10. Contours of vertical mean fluxes of the liquid−phase chemical agents fluxes at $z/H = 1$ in (a) EU05, (b) CNTL, (c) EU20, and (d) EU30. · · · 28

Figure 11. Contours of the vertical turbulent fluxes of liquid−phase chemical agents at $z/H = 1$ in (a) EU05, (b) CNTL, (c) EU20, and (d) EU30. · · · 29

Figure 12. Distributions of concentration difference of the liquid−phase chemical agents from ED00 in CNTL. · · · 32

Figure 13. Mean Surface concentrations with dry deposition velocity at the building roofs and walls. · · · 33

Figure 14. Distributions of concentration difference of the liquid-phase chemical agents from CNTL at $y/H = 0$ in (a) ED05, (b) ED20, and (c) ED50 from ED00. · 34

Figure 15. Contours of the concentrations of the (a) liquid-phase and (b) gas-phases chemical agents at $y/H = 0$ in EE05. · · · · · · · · · · · 37

Figure 16. The same as in Fig. 15 except for EE20. · · · · · · · · · · · 38

Figure 17. The same as in Fig. 15 except for EE40. · · · · · · · · · · · 39

Figure 18. The same as in Fig. 15 except for EE80. · · · · · · · · · · · 40

건성 침적 효과를 고려한 이상 화학작용제 확산 모델 개발

한 상 철

부경대학교 대학원 환경대기과학과

요 약

본 연구에서는 비반응성 이상 화학작용제의 확산 모델을 개발하였다. 개발한 확산 모델을 고해상도 전산유체역학(computational fluid dynamics, CFD) 모델과 결합하여 도시 협곡에서 이상 화학작용제의 확산 특성을 조사하였다. 도시 협곡의 풍상측 건물에서 액체상 화학작용제가 살포된다는 가정하에 액체상 화학작용제의 기화 현상을 고려하여 풍속, 증발률, 건성 침적 속도 등 다양한 환경변수들이 이상 화학작용제의 확산에 미치는 영향을 분석하였다. 유입 풍속 증가는 액체상 화학작용제 농도를 도시 협곡 위에서는 감소시키지만 도시 협곡 내부로의 유입을 증가시켜 도시 협곡 내부 농도를 증가시켰다. 건성 침적 속도가 증가할수록 풍하측 건물 근처에서 건성 침적에 의한 농도 감소가 크게 나타났다. 액체상 화학작용제의 증발율이 증가할수록 기체상 화학작용제 농도는 증가하였지만, 확산 범위는 크게 변하지 않았다. 도시 협곡에서 화학작용제 확산과 건성 침적이 유입 풍속과 증발율에 의해 크게 영향을 받을 수 있음을 확인하였다. 본 연구에서는 이상 화학작용제의 확산 모델을 개발하고 이상화된 도시 협곡에서 이상 화학작용제의 확산 특성을 조사하였다. 향후, 개발한 확산 모델 검증과 실제 도시 환경에서의 적용 가능성을 확보를 위한 추가 연구가 필요하다.

Ⅰ. Introduction

Increasing urbanization raises concerns regarding potential combat scenarios, urban warfare, and the heightened threat of terrorism employing chemical and biochemical weapons. Following the significant 9/11 attacks, substantial efforts have been dedicated to formulating strategies to counter explosive terrorism (Song and Yoon, 2012). The global trend indicates a growing utilization of biochemical agents, including chemical weapons, amplifying the risk associated with explosive terrorism. Chemical agents, encompassing toxic substances in liquid, gas, or solid states, possess the potential for direct harm to humans, animals, and plants. They are categorized into groups such as blood, asphyxiant, blister, and nerve agents, with blister and nerve agents being particularly potent and often used as military-grade chemical weapons (Choi et al., 2015). Furthermore, the dispersal capabilities of chemical agents in the form of gas, liquid, or aerosols endow them with rapid and lethal effects on humans (FOLLOWS, 2005). Notably, the Tokyo subway attack in 1995 involved the use of Sarin, a nerve agent, resulting in 12 fatalities and over 5,000 injuries (Yanagisawa et al., 2006).

Chemical agents exhibit varying dispersion and deposition effects depending on factors such as particle size, evaporation rate, and distribution coefficient. These agents are released as aerosols in the liquid or gaseous state and can either settle to the ground or remain suspended in the atmosphere, depending on their particle size. They initially form primary agent clouds and subsequently generate secondary agent clouds as they evaporate from the surface or while

suspended in the air (Kukkonen et al., 2001). Numerical modeling studies considering the deposition effects of chemical agents are relatively limited. To better understand the dispersion characteristics of chemical agents, there is a need for diffusion behavior models that account for the properties of these agents and consider deposition effects. Various military chemical and biological models, such as HPAC (Hazard Prediction and Assessment Capability) and CATS (Consequences Assessment Tool Set), have been developed and utilized in research, particularly by the U.S. DTRA (Defense Threat Reduction Agency), to assess and understand the behavior of chemical agents (DTRA, 2007). In South Korea, the Agency for Defense Development (ADD) has developed its own NBC-RAMS (nuclear, biological, and chemical reporting and modeling software system) as a military chemical and biological modeling. However, these models have low spatial resolution, limiting their ability to directly resolve buildings or other obstacles. There is a notable scarcity of research on dispersion modeling of hazardous chemical agents. Particularly, rapid urbanization has led to an increase in building height, density, and the prevalence of urban street canyons, which are spaces between buildings (Kim et al., 2015). Consequently, to conduct research on the dispersion characteristics of chemical agents in urban areas where the potential for chemical agent-based terrorism is higher, there is a critical need for high-resolution modeling systems capable of directly representing buildings. Computational Fluid Dynamics (CFD) models offer high spatial resolution to dissect complex terrain and building structures, realistically reproducing the diffusion of atmospheric pollutants at a detailed scale (Wang and Kim, 2015). The flow within urban street canyons can be influenced by meteorological conditions such as wind

speed and turbulence intensity (Kim et al., 2021; Chen et al., 2021). Additionally, it can exhibit diverse and intricate flow patterns depending on factors such as building aspect ratio, height, road width, and other conditions. While research on flow characteristics and the behavior of air pollutants in urban street canyons has been actively pursued (Vardoulakis et al., 2003; Ahmad et al., 2005; Hayati et al., 2019; Kang and Kim, 2023), studies focusing on the behavior characteristics of different chemical agents within urban street canyons are rare.

In this study, we aim to develop a diffusion model that accounts for dry deposition effects for various chemical agents and integrate it with computational fluid dynamics models to investigate the behavior characteristics of dispersed chemical agents within urban street canyons affected by evaporation on building rooftops. We assume the release of liquid-phase chemical agents from the windward side of buildings in urban street canyons and analyze the dispersion and distribution characteristics of these chemical agents under various conditions, including wind speed, evaporation rate of liquid-phase chemical agents, and dry deposition velocity.

Ⅱ. Methods

2.1. Numerical model

In this study, we employed a high-resolution computational fluid dynamics (CFD) model capable of finely resolving buildings and topography with spatial accuracies ranging from meters to tens of meters. This model can provide a detailed representation of the average motion of three-dimensional fluids in urban areas characterized by complex distributions of buildings and topography (Law et al., 2019). The CFD model used in our study adopts the k-ε turbulence closure method based on the renormalization group (RNG) theory proposed by Yakhot et al. (1992). The governing equations are the Reynolds-averaged Navier-Stokes (RANS) equations, like those used by Kim and Baik (2010). The model assumes a three-dimensional, non-rotating, incompressible, and unsteady atmospheric flow regime. It utilizes a staggered grid system and employs the finite volume method along with the semi-implicit method for pressure-linked equations (SIMPLE) algorithm for numerical integration. The Reynolds-averaged equations, the continuity equation for mass, and the transport equation for a non-reactive passive scalar are as follows.

$$\frac{\partial U_{\mathrm{i}}}{\partial t} + U_{\mathrm{j}}\frac{\partial U_{\mathrm{i}}}{\partial x_{\mathrm{j}}} = -\frac{1}{\rho_0}\frac{\partial P^*}{\partial x_{\mathrm{i}}} + \nu\frac{\partial^2 U_{\mathrm{i}}}{\partial x_j \partial x_{\mathrm{j}}} - \frac{\partial}{\partial x_{\mathrm{j}}}(\overline{u_{\mathrm{i}} u_{\mathrm{j}}}), \quad (1)$$

$$\frac{\partial U_{\mathrm{j}}}{\partial x_{\mathrm{j}}} = 0, \quad (2)$$

$$\frac{\partial C_l}{\partial t} + U_{\mathrm{j}}\frac{\partial C_l}{\partial x_{\mathrm{j}}} = \mathrm{D}\frac{\partial^2 C_l}{\partial x_j \partial x_{\mathrm{j}}} - \frac{\partial}{\partial x_{\mathrm{j}}}\left(\overline{c_l u_{\mathrm{j}}}\right) + S_{C_l} - \frac{V_d}{\Delta} C_l, \quad (3)$$

$$\frac{\partial C_g}{\partial t} + U_j \frac{\partial C_g}{\partial x_j} = D \frac{\partial^2 C_g}{\partial x_j \partial x_j} - \frac{\partial}{\partial x_j}\left(\overline{c_g u_j}\right) + S_{C_g}. \quad (4)$$

In this study, U_i represents the ith mean velocity component, P^* denotes the deviation from the mean pressure, C_l is the mass concentration of liquid-phase chemical agents in micrograms per cubic meter [$\mu g\ m^{-3}$], and C_g signifies the volume concentration of gas-phase chemical agents in parts per million by volume [ppm_v]. The variables u_i, c_l, and c_g symbolize the subgrid-scale perturbations corresponding to U_i, C_l, and C_g respectively. The last terms on the right side of equations (3) and (4) represent the removal of liquid-phase and gas-phase contaminants due to dry deposition in the vicinity of the walls of urban street canyon buildings (Kwak and Baik, 2014). V_d is the dry deposition velocity, which has been set to 0.3 m/s in this research. V_d is dependent on the size and shape of the particles and their aerodynamic properties, and it has been shown to have a relatively wide range of values in numerous prior studies. Additional information on this subject is provided in the appendix. The symbol Δ denotes the distance from the wall (Pugh et al., 2012). The dry deposition effect on building walls is considered by calculating the distance to the building wall and utilizing the average concentration of liquid-phase chemical agents along with V_d. According to Montoya et al. (2009), gas-phase chemical agents such as Sarin have a relatively low deposition velocity of 2.5×10^{-4} m s^{-1}, NH_3 at 2.5×10^{-4} m s^{-1}, Cl_2 at 1.4×10^{-4} m s^{-1}. Hence, only the dry deposition effects of liquid-phase chemical agents are considered in this research. ν and D are the turbulent diffusivity coefficients for momentum and chemical agents, respectively, and S_{C_l}

and S_{C_g} are the source/sink terms for C_l and C_g, respectively. In equations (1), (3), and (4), the Reynolds stresses and turbulent material fluxes are parameterized as follows.

$$-\overline{u_{\mathrm{i}}u_{\mathrm{j}}} = K_{\mathrm{m}}\left(\frac{\partial U_{\mathrm{i}}}{\partial x_{\mathrm{j}}} + \frac{\partial U_{\mathrm{j}}}{\partial x_i}\right) - \frac{2}{3}\delta_{ij}\mathrm{k}, \tag{5}$$

$$-\overline{cu_{\mathrm{j}}} = K_{\mathrm{c}}\frac{\partial C}{\partial x_{\mathrm{j}}}. \tag{6}$$

where, δ_{ij} is the Kronecker delta, and k represents the turbulent kinetic energy. K_{m} and K_{c} are the turbulent diffusivity coefficients for momentum and chemical agents, respectively. The RNG $\mathrm{k}-\varepsilon$ turbulence closure model employed in this study is based on the renormalization group theory and is one of the most widely used turbulence models in computational fluid dynamics. Within the framework of the RNG $\mathrm{k}-\varepsilon$ turbulence closure model, the turbulent diffusivity coefficient for momentum (K_{m}) is parameterized as follows.

$$K_{\mathrm{m}} = C_\mu\frac{k^2}{\varepsilon}, \tag{7}$$

where, C_μ is an empirical constant (= 0.0845) and ε denotes the rate of dissipation of turbulent kinetic energy. The predictive equations for turbulent kinetic energy and its dissipation rate are expressed as follows.

$$\frac{\partial k}{\partial t} + U_{\mathrm{j}}\frac{\partial k}{\partial x_{\mathrm{j}}} = -\overline{u_{\mathrm{i}}u_{\mathrm{j}}}\frac{\partial U_{\mathrm{i}}}{\partial x_{\mathrm{j}}} + \frac{\partial}{\partial x_{\mathrm{j}}}\left(\frac{K_{\mathrm{m}}}{\sigma_{\mathrm{k}}}\frac{\partial k}{\partial x_{\mathrm{j}}}\right) - \varepsilon, \tag{8}$$

$$\frac{\partial \varepsilon}{\partial t}+U_{\mathrm{j}}\frac{\partial \varepsilon}{\partial x_{\mathrm{j}}}=-C_{\varepsilon 1}\frac{\varepsilon}{k}\overline{u_{\mathrm{i}}u_{\mathrm{j}}}\frac{\partial U_{\mathrm{i}}}{\partial x_{\mathrm{j}}}+\frac{\partial}{\partial x_{\mathrm{j}}}\left(\frac{K_{\mathrm{m}}}{\sigma_{\varepsilon}}\frac{\partial \varepsilon}{\partial x_{\mathrm{j}}}\right)-C_{\varepsilon 2}\frac{\varepsilon^{2}}{k}-R. \quad (9)$$

where, σ_{k}(=0.7179), σ_{ε}(=0.7179), $C_{\varepsilon 1}$(=1.42), and $C_{\varepsilon 2}$(=1.68) are empirical constants. The final term on the right-hand side of Equation (9) represents an additional strain rate term and is defined as follows.

$$R=\frac{C_{\mu}\eta^{3}(1-\eta/\eta_{0})\varepsilon^{2}}{(1+\beta\eta^{3})k}, \quad (10)$$

$$\eta=\frac{k}{\varepsilon}\left[\left(\frac{\partial U_{\mathrm{i}}}{\partial x_{\mathrm{j}}}+\frac{\partial U_{\mathrm{j}}}{\partial x_{\mathrm{i}}}\right)\frac{\partial U_{\mathrm{i}}}{\partial x_{\mathrm{j}}}\right]^{1/2}. \quad (11)$$

The constants used in the above equations align with the values presented by Yakhot and Smith (1992).

This study considers the interaction (vaporization) between liquid-phase and gas-phase chemical agents (Chaudhary and Singh, 2020), and the source/sink terms S_{C_l} and S_{C_g} are defined as follows.

$$S_{C_l}=-\frac{C_l d_l}{R_l}, \quad (12)$$

$$S_{C_g}=-\frac{C_{lg} d_g}{R_g}+\frac{C_l d_l}{R_l}. \quad (13)$$

where, d_l and d_g represent the evaporation rate [s^{-1}] of the liquid-phase chemical agents and the condensation rate [s^{-1}] of the gas-phase chemical agents, respectively. In our study, the condensation of the gas-phase chemical agents was not considered ($d_g = 0$). R_l and R_g denote the partition coefficients for the liquid-phase and gas-phase chemical agents. To determine the emission rate of the gas-

phase chemical agents due to the vaporization of the liquid-phase agents, the following ideal gas equation was employed.

$$V = \frac{nRT}{P} \tag{14}$$

where, P denotes the gas pressure [atm], V the volume [L], n the amount of substance in moles, R the universal ideal gas (= 0.0821 L atm K^{-1} mol^{-1}), and T the temperature [K]. The value of n is determined from the mass concentration of the liquid-phase chemical agent (C_l) and the molecular weight of the chemical agent (M) as follows.

$$n = \frac{C_l}{M} \tag{15}$$

Consequently, the concentration of the gas chemical agent evaporated from the liquid-phase chemical agent under control conditions(1atm, 0℃) is calculated as follows.

$$C_g\,[\mathrm{ppm_v}] = \frac{RT}{P}\frac{C_l}{M} \times 10^{-6} \tag{16}$$

2.2. Numerical setup

In this study, numerical experiments were conducted focusing on urban street canyons, which is characterized by buildings on both sides of a road. In urban street canyon, a variety of complex atmospheric flow patterns can emerge, influenced by meteorological conditions, building geometry, heights, and road widths (Takano and Moonen, 2013; Hofman et al., 2016; Miao et al., 2021; Lu and Peng, 2023). This study considered the same building configuration as the wind tunnel experiment by Gromke et al. (2008). The building height (H) and width (W) were set at 18 m. The building length (L) was 10H, and the street canyon width (S) was 1H, resulting in a building length-to-height ratio of 10. To meet the guidelines of COST Action 732, the numerical domain was configured with distances to the upwind boundary of 8H, the downwind boundary of 30H, the lateral boundaries of 10H, and the top boundary of 8H (Fig. 1). The grid counts in the x, y, and z directions were 500, 120, and 100, respectively, utilizing a uniform grid with grid sizes of 1.5 m, 4.5 m, and 1.5 m in each direction. The time interval was set at 0.5 seconds, and the numerical integration was conducted for a total duration of 3600 seconds. The inflow boundary conditions for wind, turbulent kinetic energy, and the rate of dissipation of turbulent kinetic energy were as follows.

$$U(z) = U_{ref}\left(\frac{z}{z_{ref}}\right)^{\alpha}, \tag{17}$$

$$V(z) = 0, \tag{18}$$

$$W(z) = 0, \tag{19}$$

$$k = \frac{{u_*}^2}{\sqrt{C_\mu}}\left(1 - \frac{z}{\delta}\right). \tag{20}$$

$$\varepsilon = \frac{{u_*}^3}{\kappa z}\left(1 - \frac{z}{\delta}\right). \tag{21}$$

where, U_{ref} denotes the wind speed at the reference height (z_{ref}), which is 18 m. The friction velocity (u_*) is set to 0.5 m s^{-1}, and C_μ is an empirical constant valued at 0.0845. The von Karman constant (κ) is assumed as 0.4, δ represents the boundary layer thickness measured at 75 m, and z_0 is the roughness length, which is established at 0.05 m.

In this study, it is assumed that liquid-phase chemical agents are dispersed from a location on the upwind-facing side of the building and within the central part of the urban street canyon (Fig. 2). The emission rate for the liquid-phase chemical agents is set at 2.02 kg s^{-1}, matching the release rate employed by Hanna et al. (2009) in their research modeling chemical dispersion following an actual explosion incident. The turbulent Schmidt number (Sc_t), which determines the turbulence diffusion coefficients for both the liquid and gas-phase chemical agents, is set to 0.3. The turbulent Schmidt number is a dimensionless quantity representing the ratio of the atmospheric turbulence-driven momentum diffusion coefficient to the mass diffusion coefficient, as detailed by Wang and Kim (2015).

This study examines the effects of ambient wind speed, dry deposition of chemical agents, and the evaporation rate of chemical agents on the concentration distribution of chemical agents around

urban street canyon. Initially, a control experimental simulation (control run, CNTL) was conducted. In the CNTL, the reference wind speed (U_{ref}) was set to 4.7 m s^{-1}, the dry deposition effect was considered, and the evaporation rate of the liquid-phase chemical agent (d_l) was set to 0.05 s^{-1}. To investigate the impact of ambient wind speed, U_{ref} was adjusted to 0.5 (below, EU05), twice (EU20), and three times (EU30) that of the CNTL. Numerical experiments were conducted to assess the effect of dry deposition by setting the dry deposition velocity (V_d) to 0 times (ED00, which excludes dry deposition), 0.5 times (ED05), twice (ED20), and four times (ED40) the rate used in the CNTL. To analyze the influence of the evaporation rate (d_1) of the liquid-phase chemical agent, experiments were performed with the evaporation rate set to 0.5 times (EE05), twice (EE20), four times (EE40), and eight times (EE80) that of the control experiment.

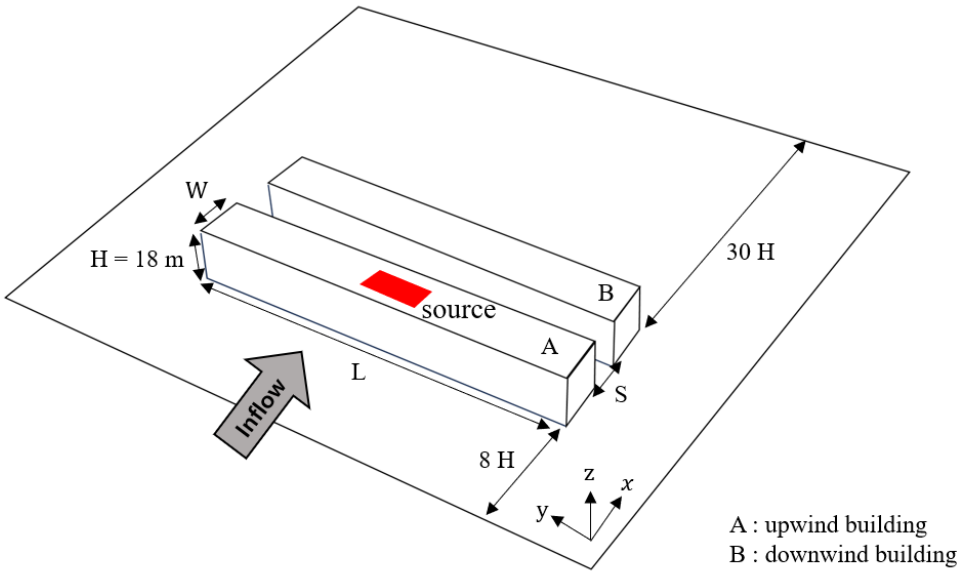

Figure 1. The numerical domain and building configuration used in this study.

Ⅲ. Results and discussion

3.1. Control Experiment

The study performed an analysis of the flow characteristics within the urban street canyon and the distribution characteristics of the non-reactive chemical agents for the control experiment. Figure 2 illustrates the wind vector field and normalized wind speed distribution in the x-z plane at $y/H = 0$. The flow pattern within the urban street canyon is greatly dependent on the aspect ratio of the street canyon, defined by the ratio of the canyon's height to its width. When the aspect ratio is 1, a single primary vortex is formed, which corresponds to a skimming flow (Di Bernardino et al., 2015; Park et al., 2015; Chew and Norford, 2018). The results of this study are consistent with previous research, showing that the flow descends along the downwind building wall and heads toward the upwind building near the canyon floor, rising along the upwind building wall. Near the roof of the upwind building, flow separation occurs as the flow entering the urban street canyon collides with the upwind building, forming a recirculation zone above the building. Along the upper boundary of the recirculation zone, the flow descends, resulting in a dominant downdraft at the roof level of the urban street canyon.

In the upwind region ($-0.5 \leq x/H \leq 0$), updrafts are prevalent, while in the downwind building region ($0 \leq x/H \leq 0.5$), downdrafts are primarily observed. Within the lower layers of the urban street canyon ($z/H \leq 0.6$), a reverse flow opposite to the inflow direction is evident. This lower layer reverse flow ascends near the upwind building,

creating vortices within the canyon (Wang and Kim, 2015). To analyze the flow around the urban street canyon in three dimensions, streamlines starting from within the canyon (z/H = 0.16, 0.33) were investigated (Fig. 4). Inside the urban street canyon, some parts of the flow escape near the building edges (indicated by the yellow circle), while others form a recirculation zone above the upwind building (recirculation zone in Fig. 2). In the central area of the urban street canyon, the flow can be seen to escape the canyon by repeating a cycle of ascending and descending movements.

Figure 4 illustrates the distribution of both liquid and gas chemical agents. While most of the liquid chemical agent dispersed from the rooftop of the upwind building is transported downwind by the ambient wind, a portion infiltrates the urban street canyon. For gas chemical agents, significant concentrations appear in areas with high liquid chemical agent concentrations due to evaporation; however, in areas where the liquid chemical agent concentration is low (below 10 g m^{-3}), the concentration of gas chemical agents is observed to be less than 1.622×10^{-7} ppb_v. Consequently, the concentration of gas chemical agents inside the urban street canyon was very low. A quantitative comparison of the average concentrations inside the urban street canyon revealed that the liquid chemical agent had a concentration of 10.56 g m^{-3}, and the gas chemical agent had a concentration of 0.896×10^{-7} ppb_v. According to Kye et al. (2008), the inhalation lethal concentration of a chemical agent known as Sarin is approximately 70 mg m^{-3}. Based on the control experiment results, the liquid chemical agent demonstrated concentrations within the urban street canyon that could result in significant human casualties.

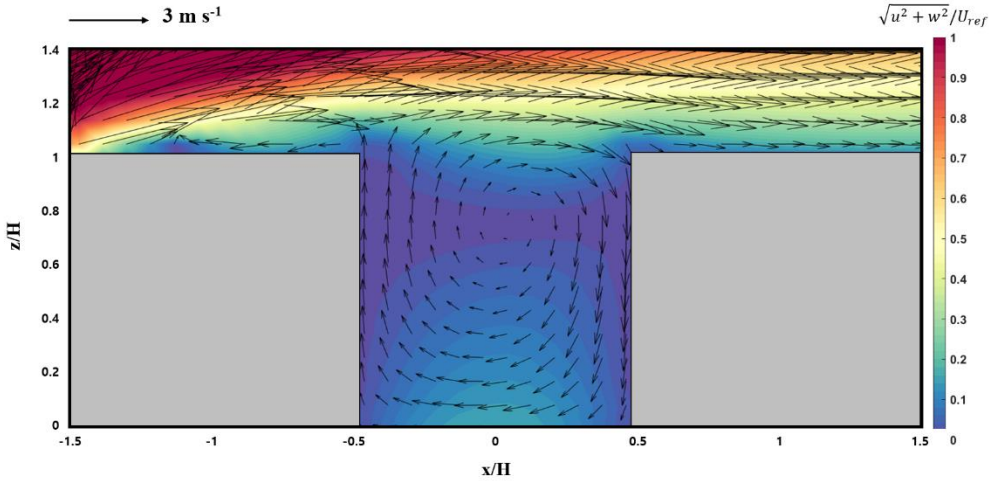

Figure 2. Wind vectors and contours of the wind speeds normalized by U_{ref} at $y/H = 0$ in CNTL.

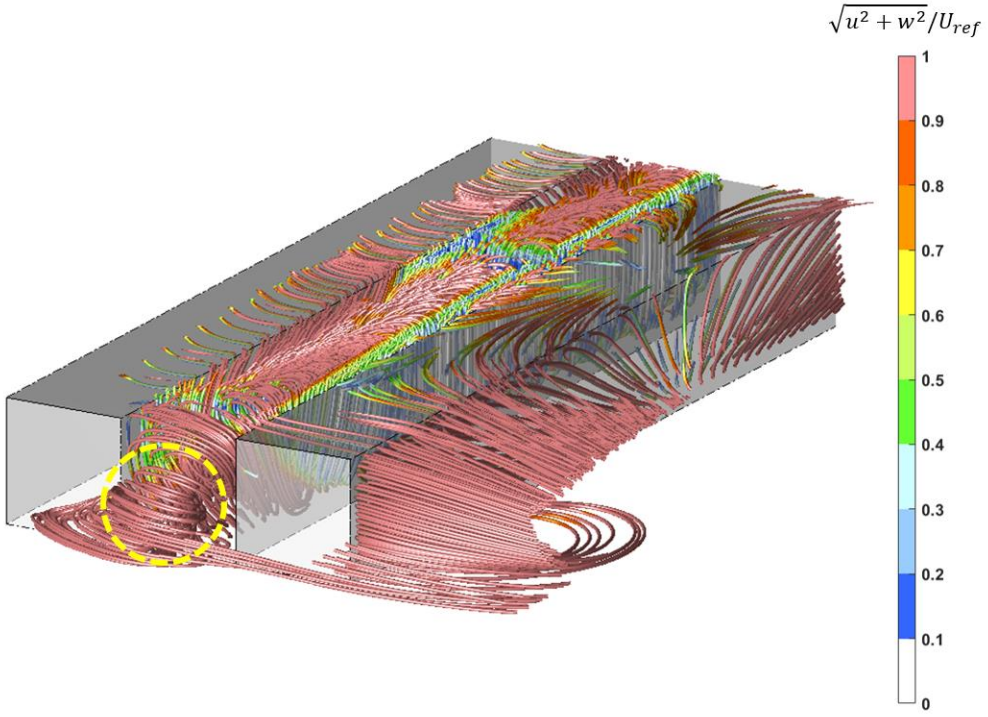

Figure 3. Streamlines starting at $z/H = 0.16$ and 0.33 around the street canyon. Colors indicate the wind speeds normalized by U_{ref}.

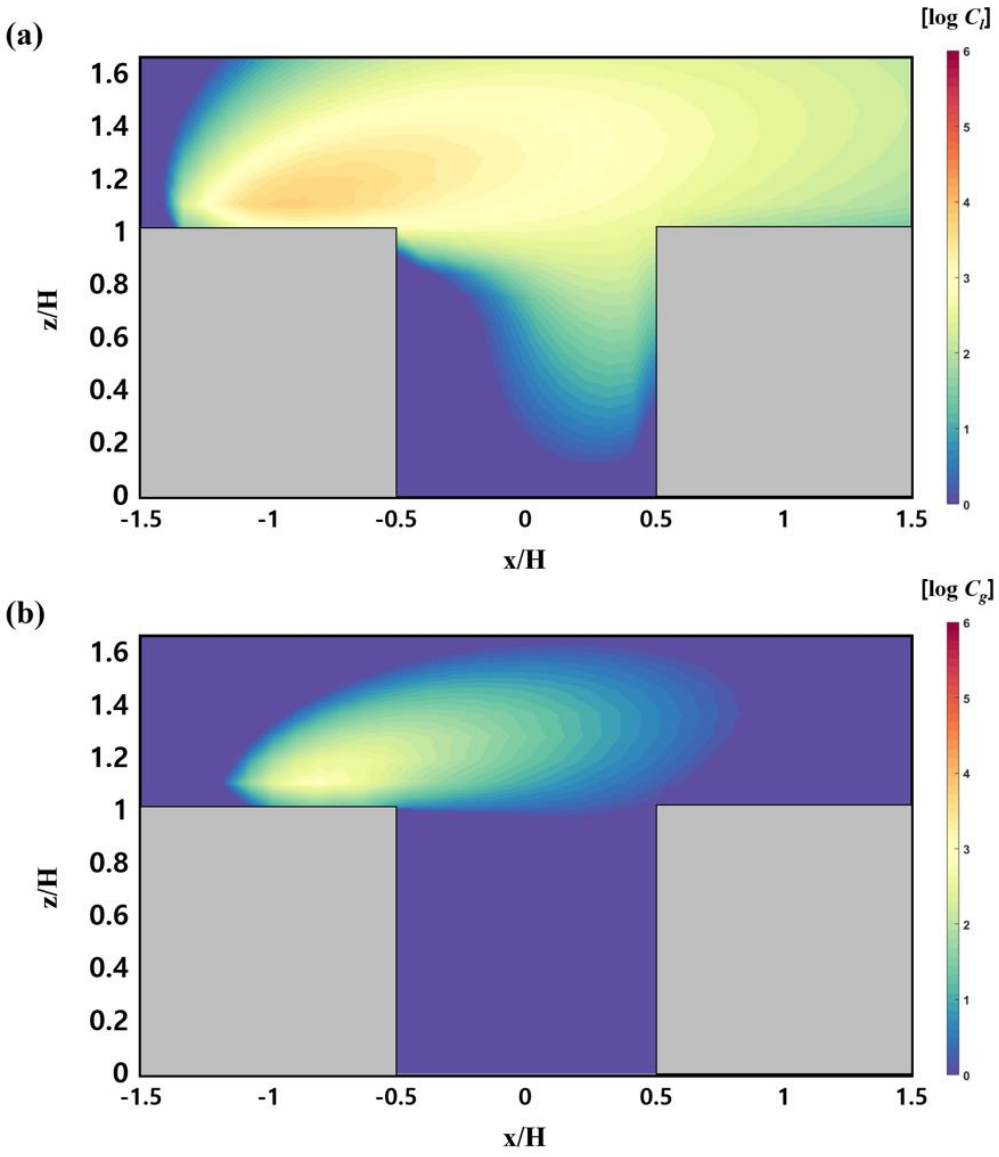

Figure 4. Contours of the concentrations of the (a) liquid− and (b) gas−phase chemical agents at $y/H = 0$ in CNTL.

Figure 5 illustrates the distribution of liquid and gas-phase chemical agents dispersed from the center of the urban canyon. Although released from the central part of the canyon, the concentrations within the canyon accumulate near the upwind building due to the flow patterns generated within the street canyon. In the case of gas-phase chemical agents, relatively high concentrations were observed in areas with high liquid-phase chemical agent concentrations, but in most cases, the concentrations were low. Quantitatively comparing the average concentrations within the urban canyon, liquid-phase chemical agents showed a concentration of 41.35 g m^{-3}, while gas-phase chemical agents exhibited a concentration of 2.3×10^{-7} ppb_v. Whether dispersed upwind or within the urban canyon, liquid-phase chemical agents both demonstrated concentrations within the urban canyon that could result in significant human casualties.

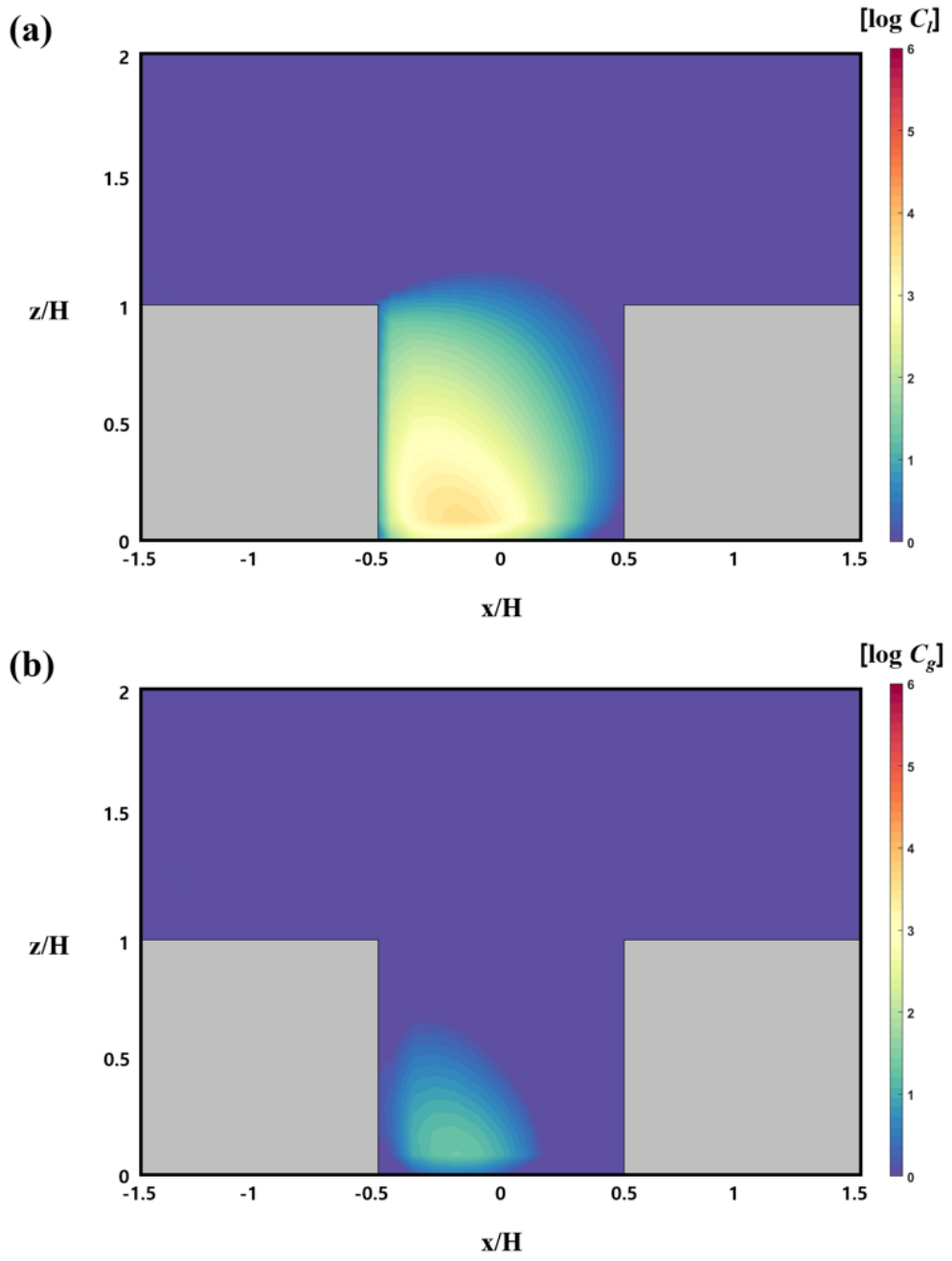

Figure 5. When a source is located within the street canyon, contours of the concentrations of the (a) liquid−phase and (b) gas−phase chemical agents at $y/H = 0$ in CNTL.

3.2. Effects of the ambient wind speeds

This research utilizes a dispersion model for non-reactive chemical agents to examine the distribution of chemical agent concentrations in relation to changes in ambient wind speed. Numerical experiments were conducted setting the inflow wind speed at the reference height (U_{ref}) to half (EU05), double (EU20), and triple (EU30) the control experimental condition (CNTL). Figure 6 illustrates the streamline distribution, indicating that as U_{ref} increases, the size of the recirculation zone behind the downwind building enlarges, yet the internal flow pattern within the urban street canyon remains consistent (as shown in Fig. 6). Figure 7 displays the dimensionless wind vector field and wind speed distribution on the x-z plane. Similar to the CNTL condition, the flow ascends along the downwind building wall and encounters flow separation near the rooftop of the upwind building, where it then contributes to forming a recirculation zone. With the increase in U_{ref}, the size of the recirculation zone expands, with the flow descending along the upper boundary of the recirculation area. Figure 8 presents the distribution of liquid-phase chemical agent dispersion at the center of the urban street canyon ($y/H = 0$) as ambient wind speed changes. For liquid-phase chemical agents, as the inflow intensity strengthens, concentrations above the urban street canyon decrease, while the influx and concentration of liquid-phase chemical agents within the urban street canyon increase. As depicted in Figure 7, with the increase of U_{ref}, the descending flow along the upper boundary of the recirculation zone above the upwind building intensifies, leading to an increased concentration of liquid-phase

chemical agents being transported into the urban street canyon. Figure 9 shows the distribution of gas−phase chemical agent dispersion at the center of the urban street canyon ($y/H = 0$) as a function of changes in ambient wind speed. Similar to the liquid−phase chemical agents, as the inflow intensity strengthens, the concentration of gas−phase chemical agents decreases above the urban street canyon while increasing within it.

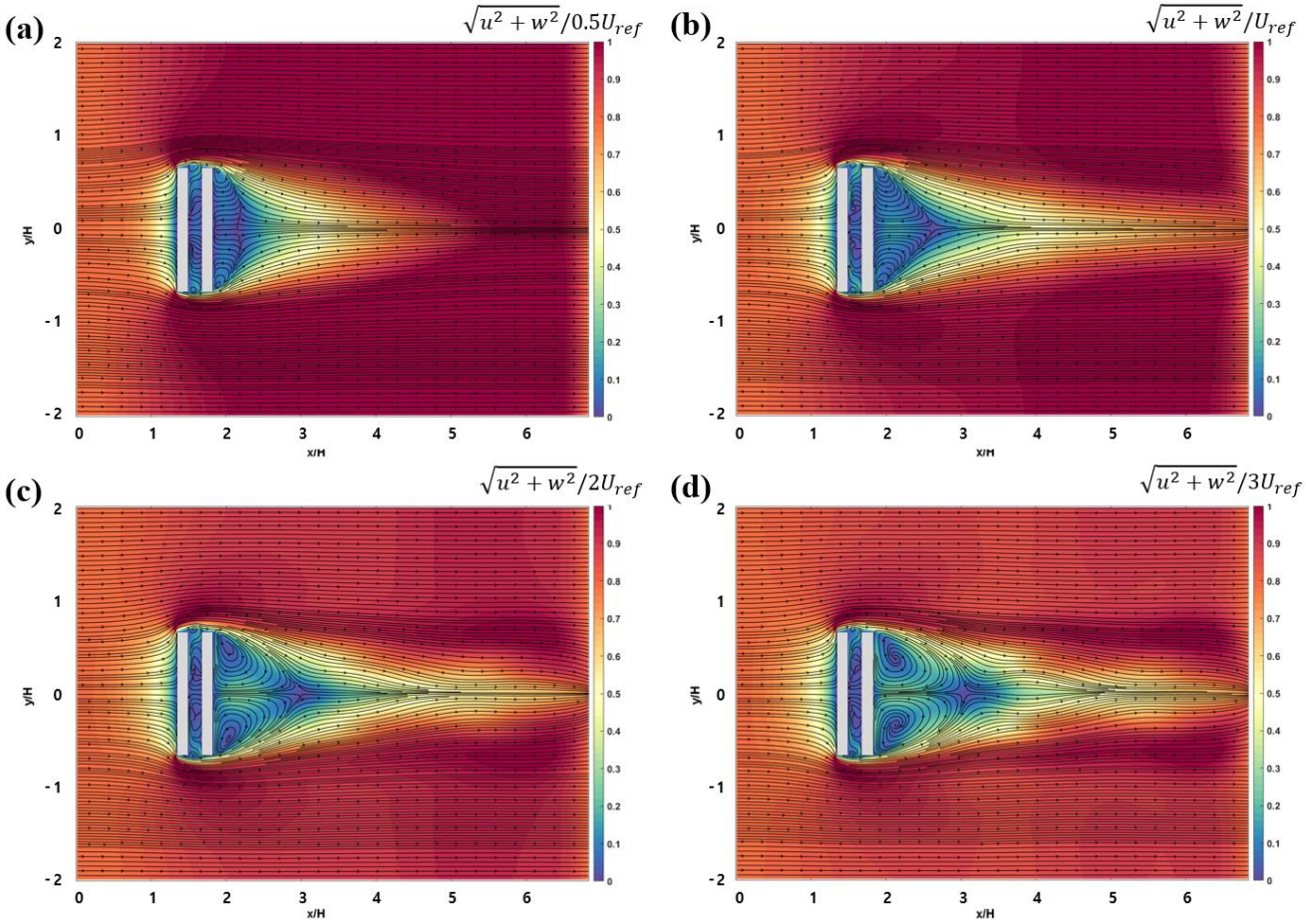

Figure 6. Streamlines and contours of wind speeds normalized by U_{ref} at $z/H = 0.5$ in (a) EU0.5, (b) CNTL, (c) EU20, and (d) EU30.

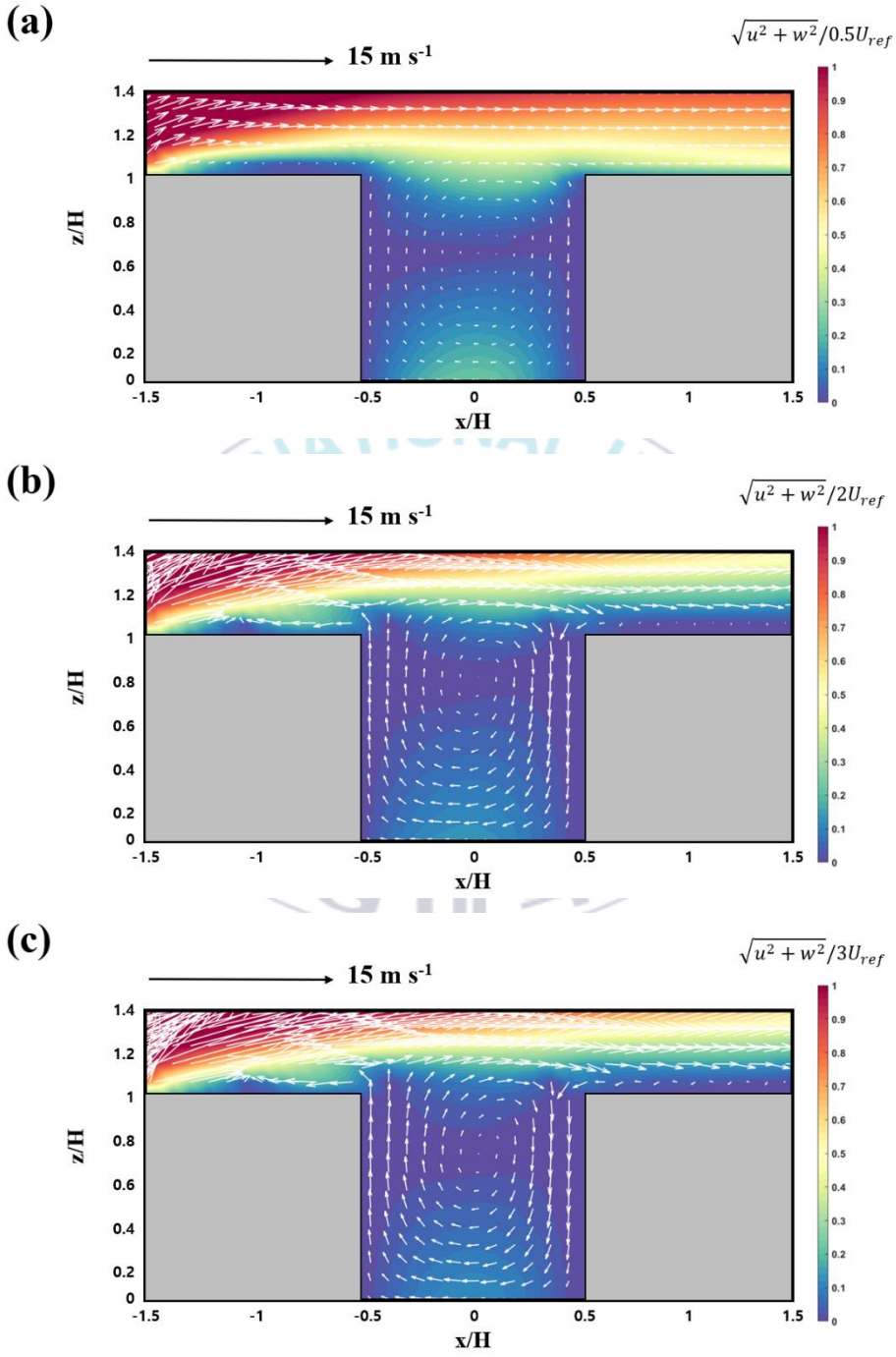

Figure 7. Wind vectors and contours of the wind speeds normalized by U_{ref} at $y/H = 0$. in (a) EU0.5, (b) EU20, and (c) EU30.

The vertical fluxes of chemical agents at the roof level of the urban street canyon due to mean flow and turbulence have been investigated. The mean fluxes (Q_c) due to the mean flow and the turbulent diffusion fluxes (Q_t) are defined as follows.

$$Q_m = WC, \tag{22}$$

$$Q_t = -\overline{wc} \tag{23}$$

where, C and c represent the mean concentration of the chemical agent and the deviation from the mean, respectively. Figure 10 illustrates the distribution of mean fluxes of liquid-phase chemical agents at the roof level of the urban street canyon ($z/H = 1$) due to mean flow, as the ambient wind speed varies. As the ambient wind speed increases, the downward currents strengthen, resulting in an increased influx of liquid-phase chemical agent fluxes into the urban street canyon. The liquid-phase chemical agents that enter the canyon are transported towards the upwind building by reverse flow in the lower region ($z/H < 0.5$) and then conveyed upwards along the building wall. For the gas-phase chemical agents produced by the evaporation of the liquid-phase agents (d_l = 0.05), relatively low concentrations were observed within the canyon; however, the concentration inside the canyon increased as U_{ref} increased. Figure 11 depicts the distribution of turbulent fluxes of liquid-phase chemical agents at the roof level of the urban street canyon ($z/H = 1$), in response to changes in ambient wind speed. An analysis of the turbulent diffusion fluxes distribution at the roof level ($z/H = 1$) indicated that, as U_{ref} intensified, turbulent diffusion fluxes diminished. This decrease in

turbulent diffusion fluxes with stronger U_{ref} is attributed to an increase in the turbulent diffusion coefficient at roof level $(z/H = 1)$, an amplified turbulent diffusion coefficient on the upwind side, and a reduced turbulent diffusion coefficient on the downwind side of the building. Consequently, the concentration gradient between the chemical agents above the roof level and within the urban street canyon decreases due to an increase in fluxes caused by mean flow.

Averaging the concentrations of liquid-phase chemical agents within the urban street canyon at the center $(y/H = 0)$, the mean concentrations for EU05, CNTL, EU20, and EU30 were 2.52, 3.96, 7.37, and 8.99 g m^{-3}, respectively. Similarly, averaging the concentrations of gas-phase chemical agents within the urban street canyon at the center (y/H =0), the mean concentrations for EU05, CNTL, EU20, and EU30 were 4.53×10^{-8}, 7.11×10^{-8}, 1.33×10^{-7}, 1.622×10^{-7} ppb_v, respectively.

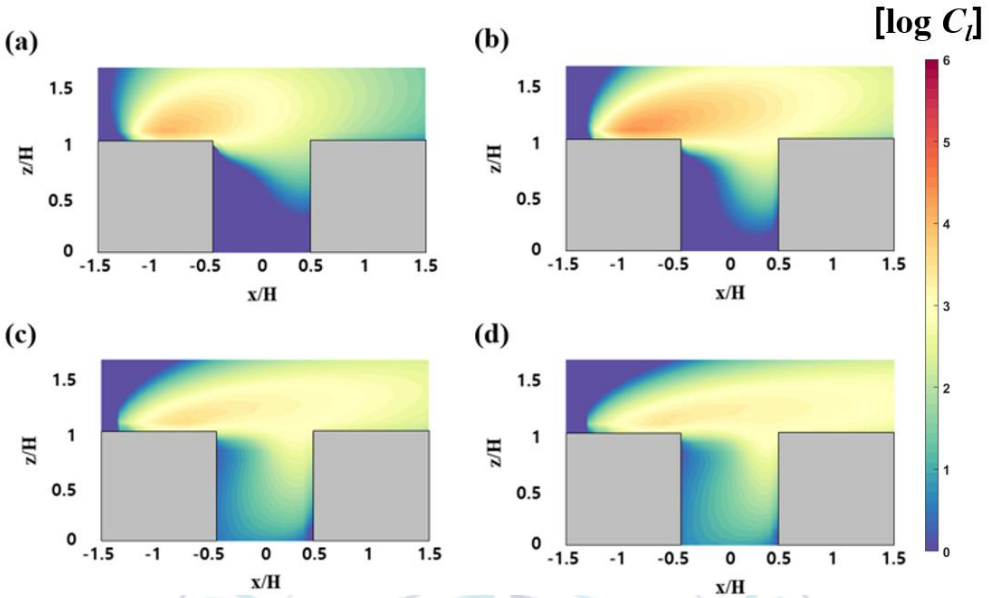

Figure 8. Contours of the concentrations of the liquid-phase chemical agents at $y/H = 0$ in (a) EU05, (b) CNTL, (c) EU20, and (d) EU30.

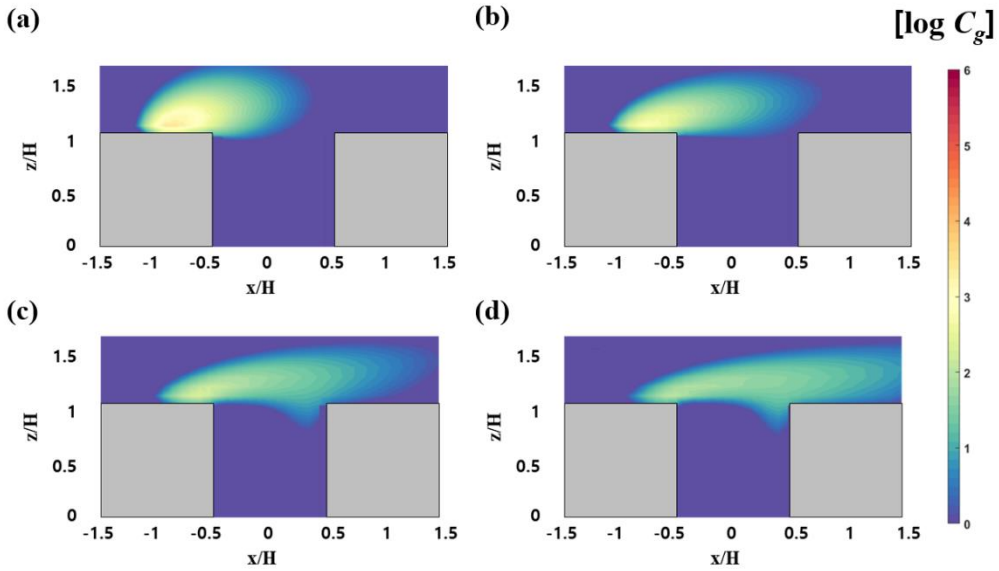

Figure 9. The same as in Fig. 8 except for the gas-phase chemical agents.

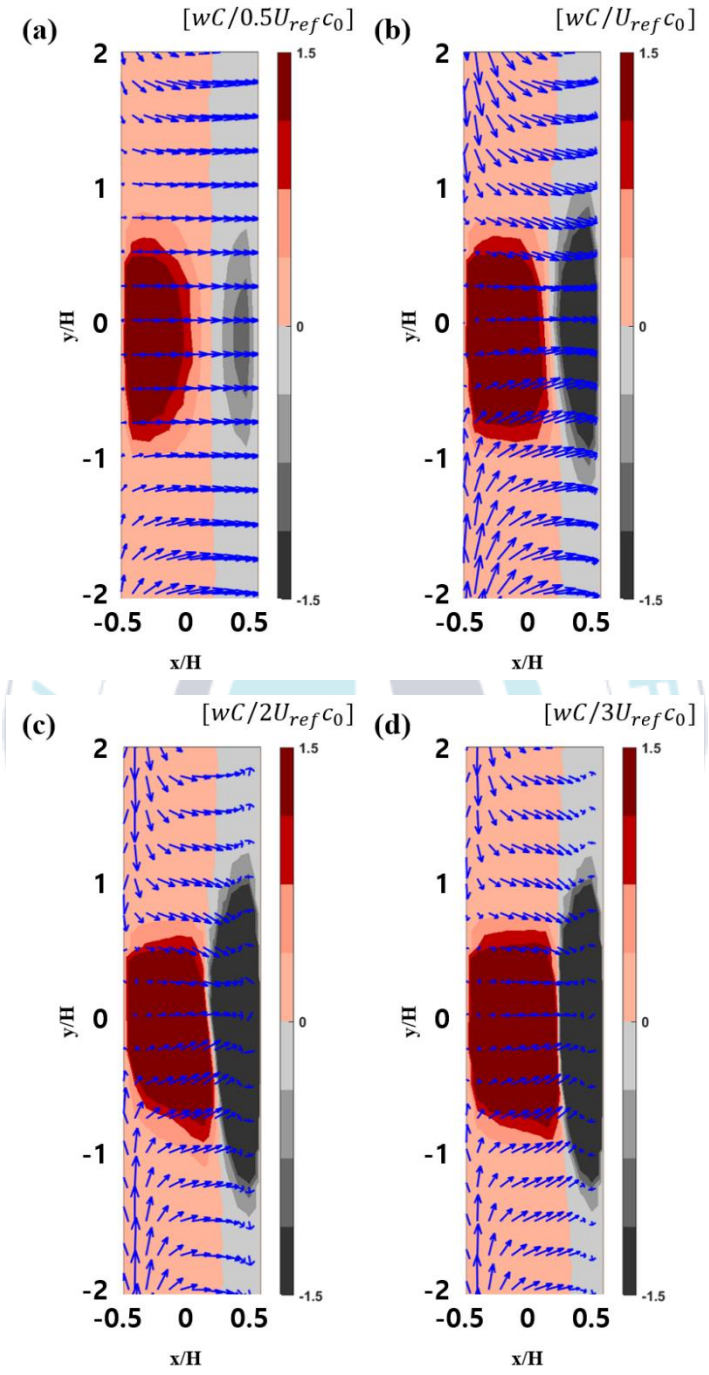

Figure 10. Contours of vertical mean fluxes of the liquid-phase chemical agents fluxes at $z/H = 1$ in (a) EU05, (b) CNTL, (c) EU20, and (d) EU30.

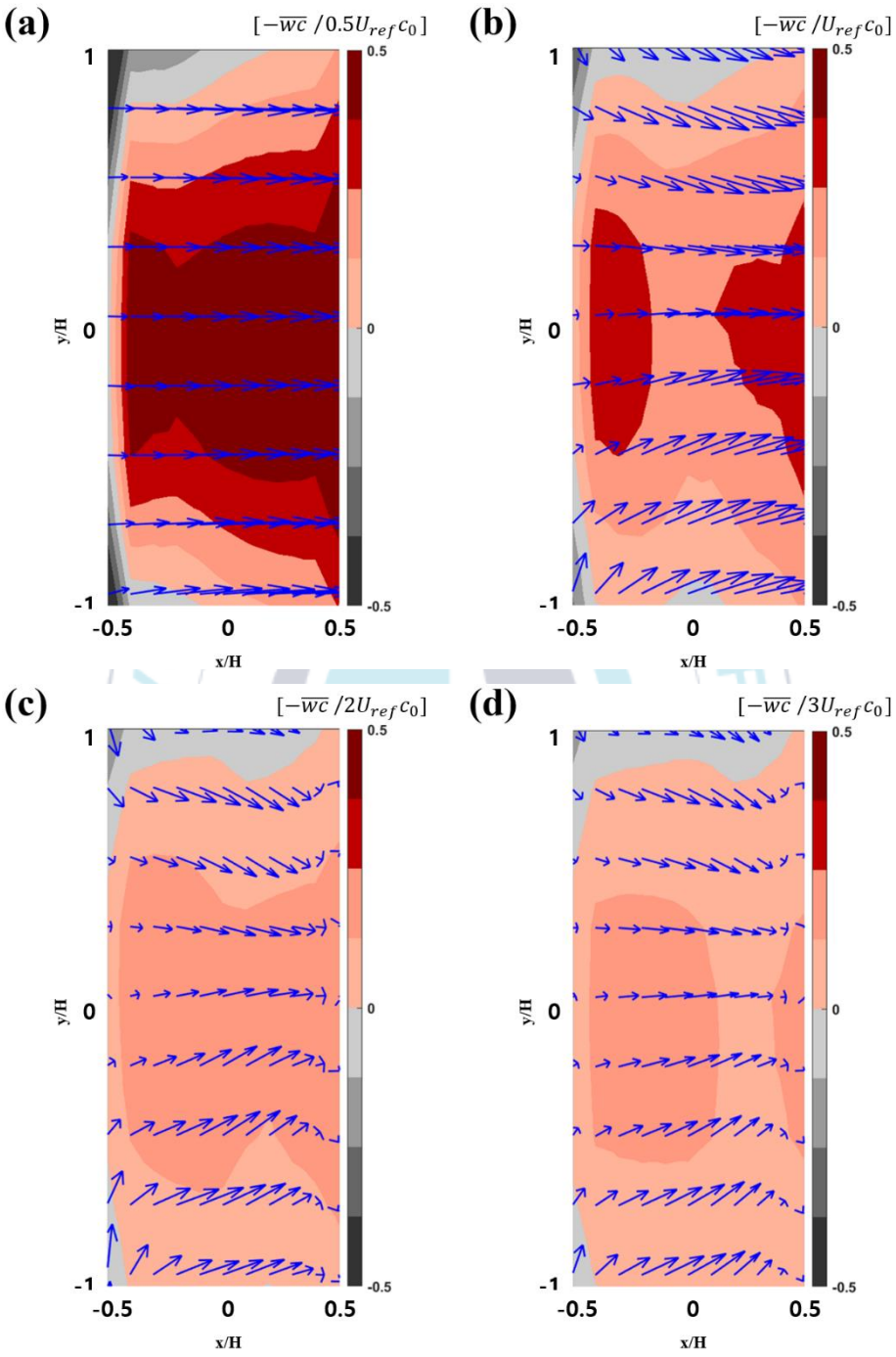

Figure 11. Contours of the vertical turbulent fluxes of the liquid-phase chemical agents at $z/H = 1$ in (a) EU05, (b) CNTL, (c) EU20, and (d) EU30.

3.3. Effects of the dry deposition

The study analyzed the effect of dry deposition on the dispersion of liquid-phase chemical agents by varying the dry deposition velocity (V_d). Based on Montoya et al. (2009), the dry deposition velocities for gas-phase chemical agents such as Sarin are relatively low, at 2.5×10^{-4} m s^{-1} for Sarin, 2.5×10^{-4} m s^{-1} for NH_3, and 1.4×10^{-4} m s^{-1} for Cl_2, and hence were not considered in this research for gas-phase chemical agents. Numerical experiments were conducted with the dry deposition velocity (V_d) set at zero (ED00), excluding dry deposition effect), at half (ED05), twice (ED20), and four times (ED40) the control experiment dry deposition velocity. Initially, the control experiment results for liquid-phase chemical agents were compared with the ED05 results. Figure 12 illustrates the concentration difference distribution between CNTL and ED00. Near the downwind building wall within the urban street canyon, a maximum concentration decrease of 6.97 g m^{-3} was observed. The study further analyzed the average concentration changes of liquid-phase chemical agents from the ground up to the roof height along the downwind building wall area within the urban street canyon. As the dry deposition velocity increased, a decrease in the concentration of liquid-phase chemical agents was observed in the respective wall areas, with concentrations dropping to 11.13 g m^{-3} for ED05, 5.93 g m^{-3} for ED20, and 4.13 g m^{-3} for ED40. The average concentration at the upwind building wall showed 10.08 g m^{-3} for ED05, 7.62 g m^{-3} for ED20, and 6.48 g m^{-3} for ED40. Figure 13 represents the mean concentrations at the upwind building wall, the downwind building wall, and the roof height. An exponential decrease

in average concentration was evident with increasing dry deposition velocities. Figure 14 compares the concentration differences of liquid-phase chemical agents for ED05, ED20, and ED40 with the control experiment ED00, illustrating an increase in concentration difference (indicating an increased effect of dry deposition) with higher dry deposition velocities. While the increase in dry deposition velocity resulted in a significant decrease in the concentration of chemical agents near the downwind building, the concentration differences near the upwind building wall were not as pronounced, reflecting the less concentrated distribution of liquid-phase chemical agents influenced by urban street canyon vortices and their initial lower concentrations at the upwind wall.

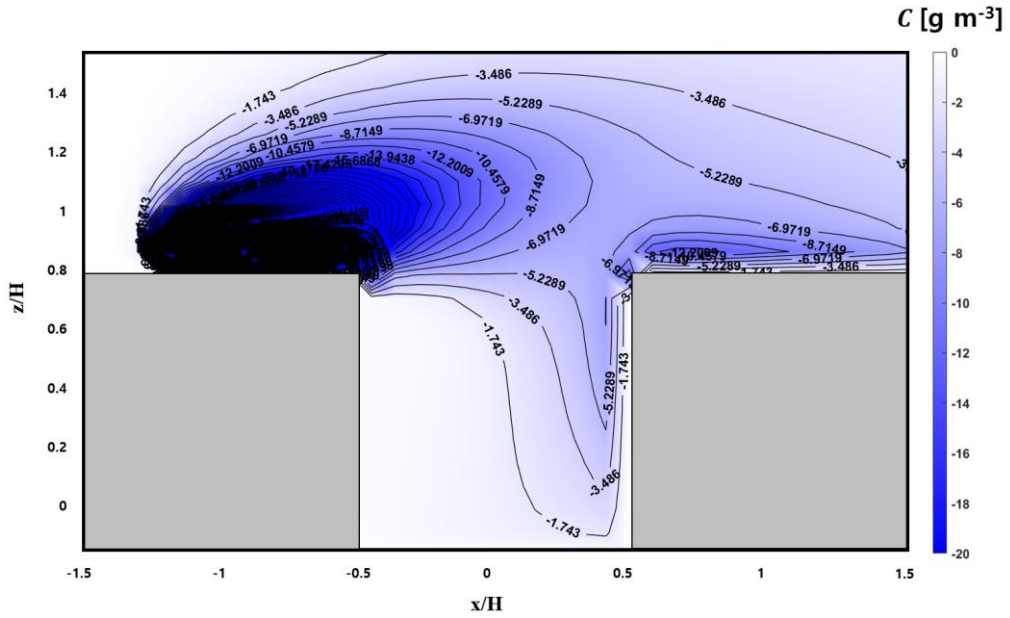

Figure 12. Distributions of concentration difference of the liquid-phase chemical agents from ED00 in CNTL.

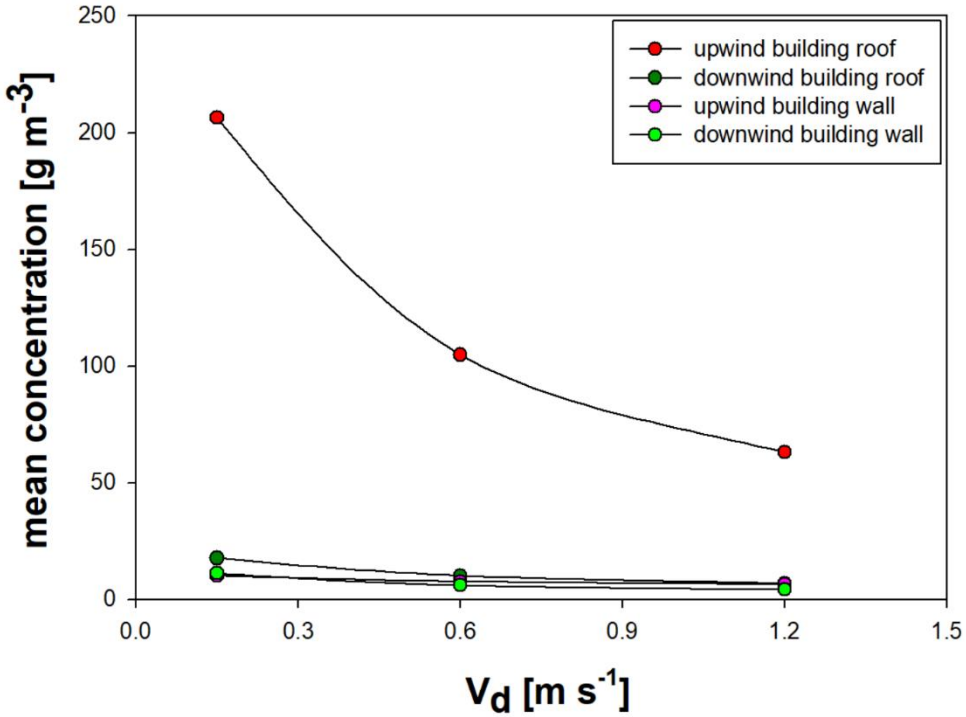

Figure 13. Mean surface concentrations with dry deposition velocity at the building roofs and walls.

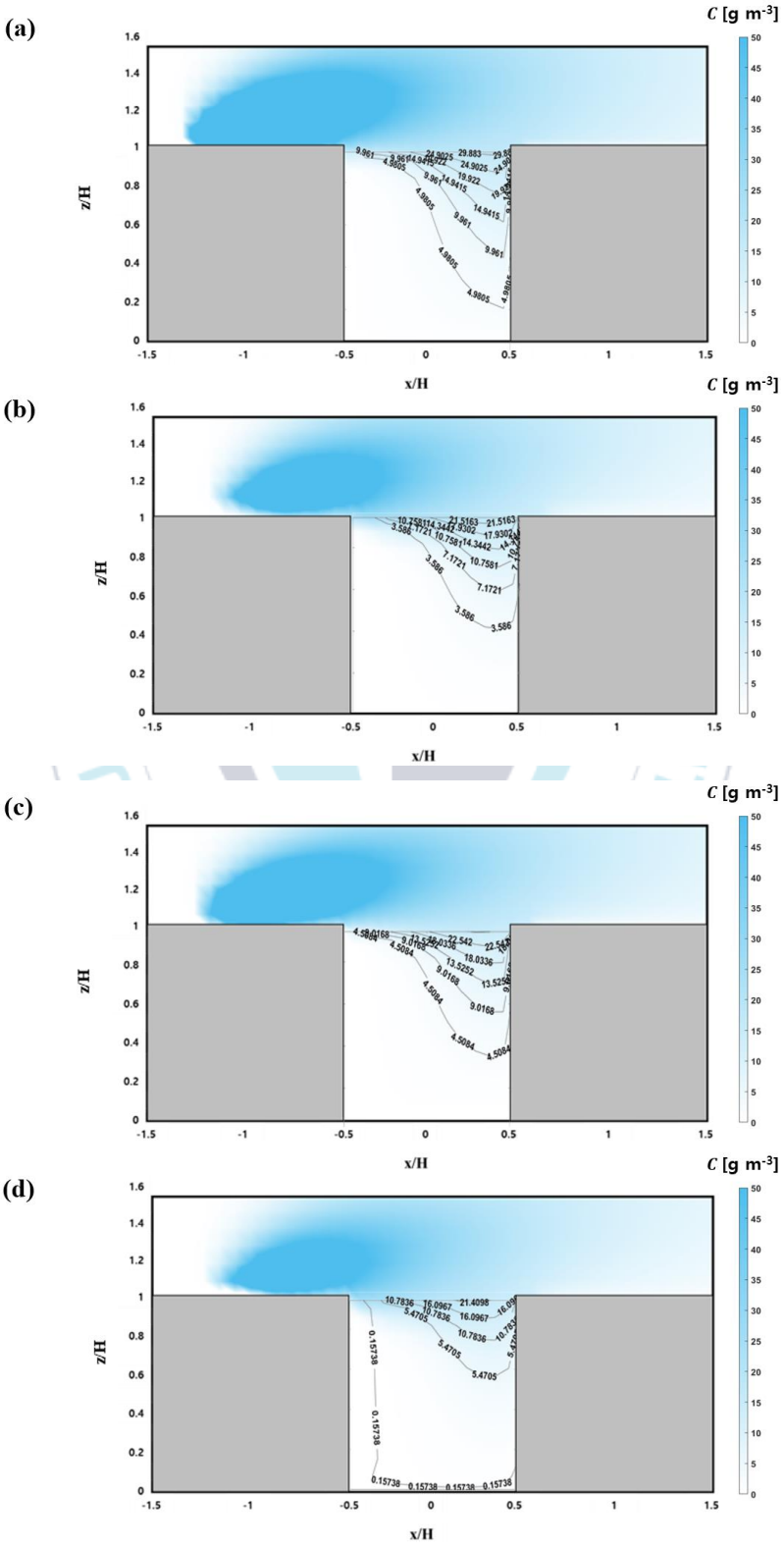
(a)
C [g m-3]
z/H
x/H
(b)
C [g m-3]
z/H
x/H
(c)
C [g m-3]
z/H
x/H
(d)
C [g m-3]
z/H
x/H

Figure 14. Distributions of concentration difference of the liquid-phase chemical agents from CNTL in at $y/H = 0$ in (a) ED00, (b) ED05, (c) ED20, and (d) ED40 from ED00.

3.4. Effects of the Evaporation rate

The influence of the evaporation rate of liquid-phase chemical agents (d_l) was analyzed (Figs. 15—18). As the evaporation rate increased, a decrease in the concentration of liquid-phase chemical agents and a rise in the concentration of gas chemical agents were observed. In EE05 and EE20, liquid-phase chemical agents were introduced into the urban street canyon; however, in EE40 and EE80, where the evaporation rate was higher, a significant amount of the liquid-phase chemical agents dispersed from the upwind building evaporated before entering the canyon, resulting in very low concentrations. The concentration of liquid-phase chemical agents entering the canyon in EE05 was higher than that in CNTL, while the concentration of gas chemical agents was lower. All experiments with varied evaporation rates showed an influx of gas chemical agents into the urban street canyon, but the amount was minimal.

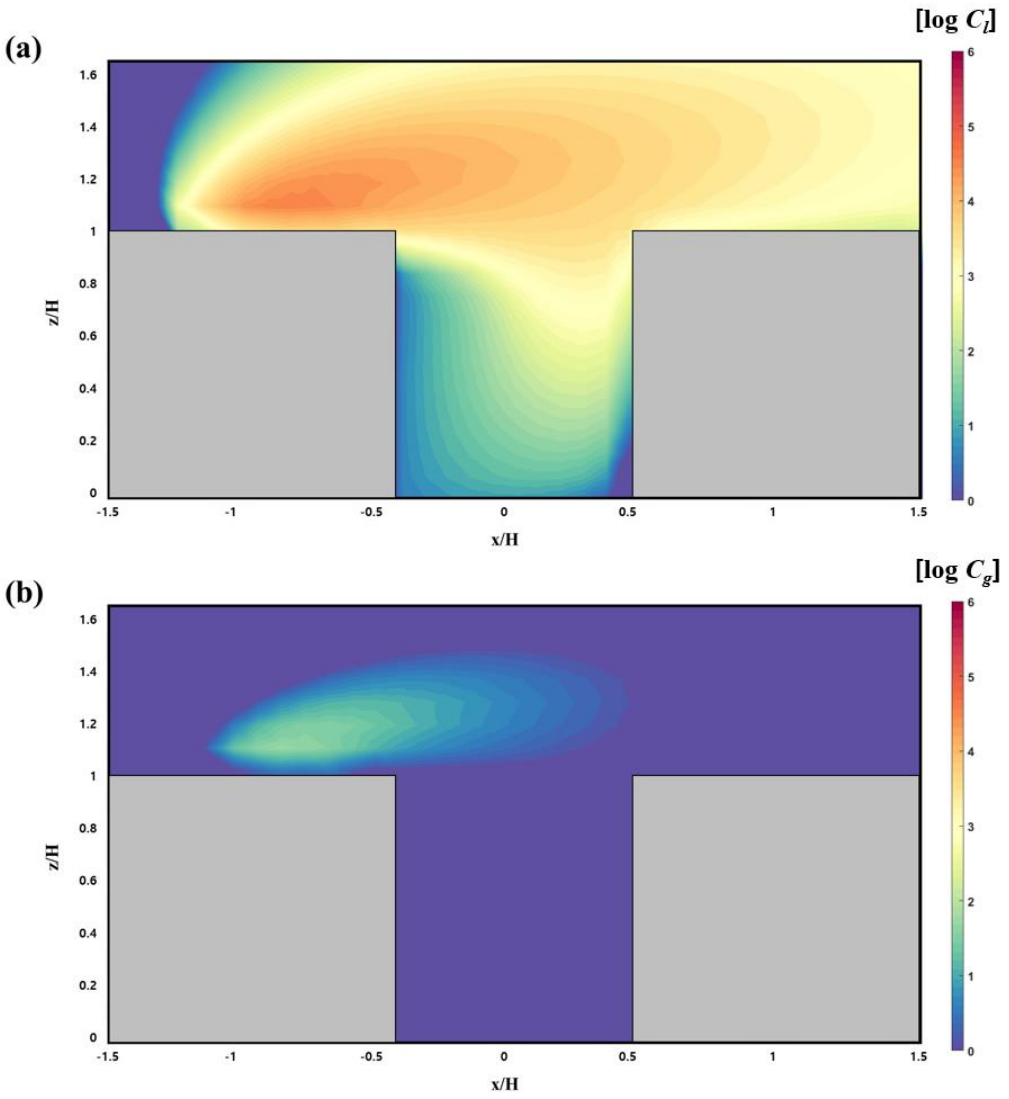

Figure 15. Contours of the concentrations of the (a) liquid−phase and (b) gas−phases chemical agents at $y/H = 0$ in EE05.

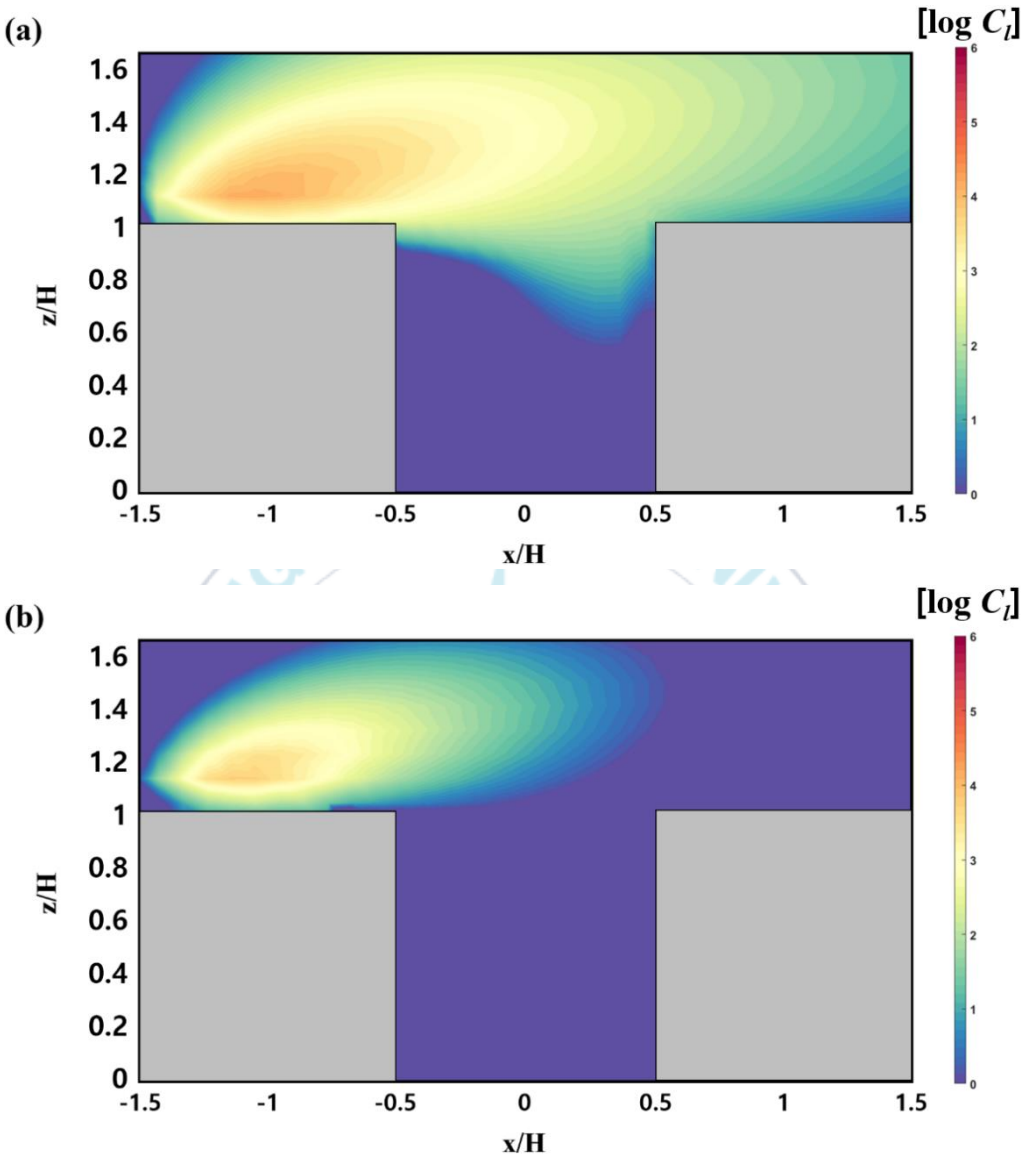

Figure 16. The same as in Fig. 15 except for EE20.

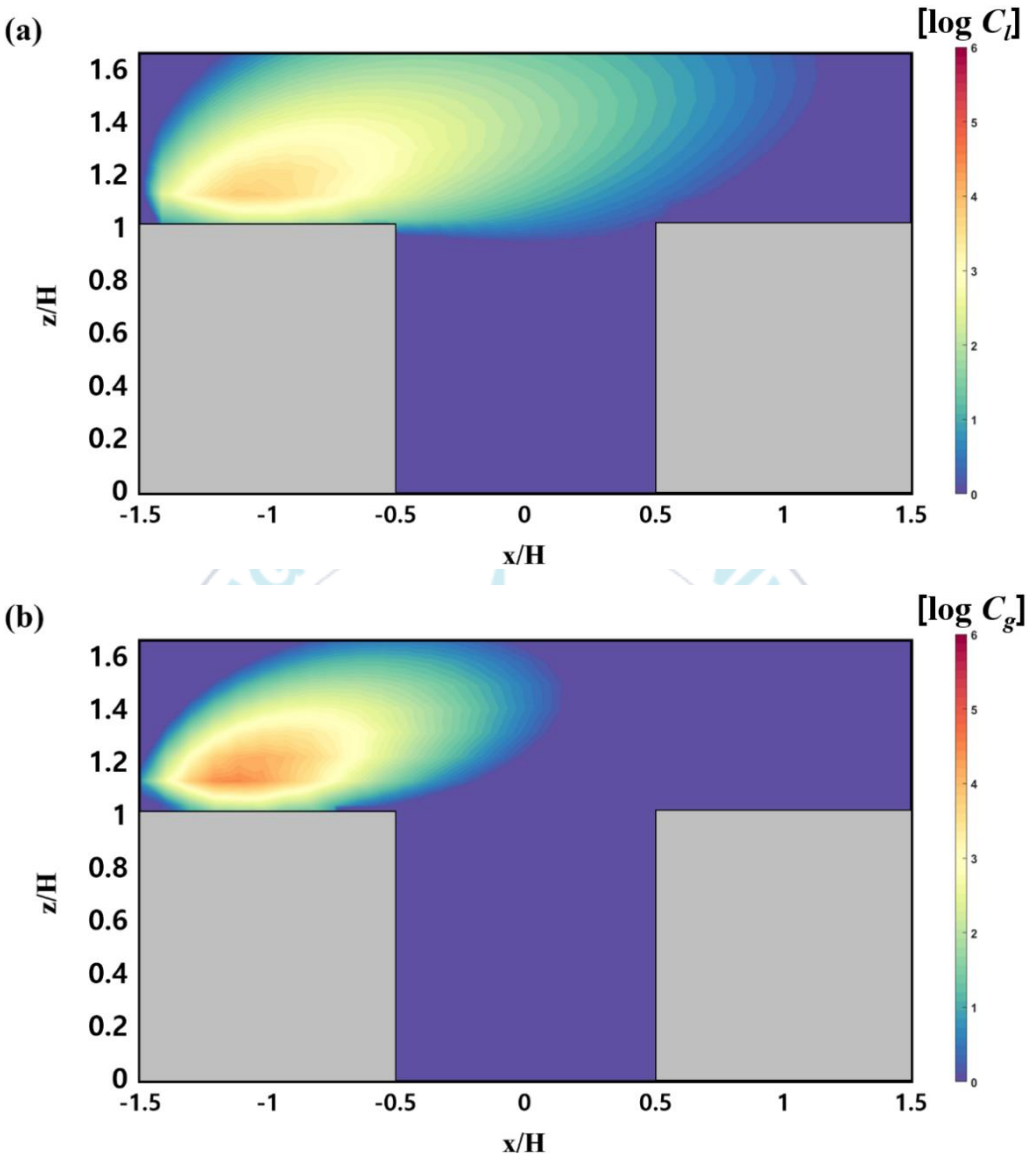

Figure 17. The same as in Fig. 15 except for EE40.

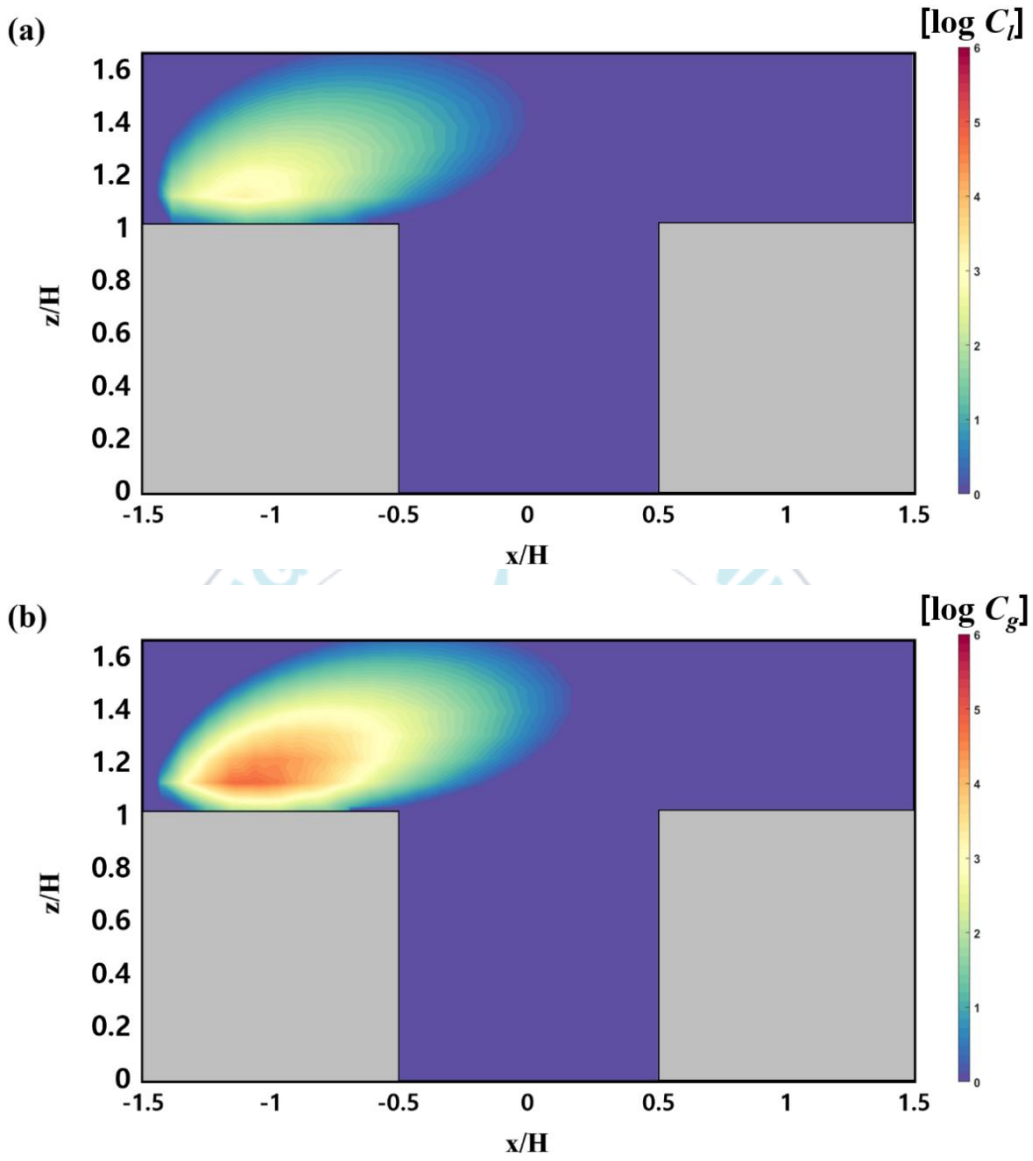

Figure 18. The same as in Fig. 15 except for EE80.

Ⅳ. Summary and Conclusions

In this study, a dispersion model for non-reactive chemical warfare agents was developed and integrated with a computational fluid dynamics (CFD) model to investigate the dispersion characteristics of such agents in urban street canyons. Assuming the dispersion of liquid-phase chemical warfare agents from the central part of the urban street canyon and the upwind building, we varied environmental factors such as wind speed, evaporation rate, and dry deposition velocity to analyze their effects.

An increase in the incoming wind speed reduced the concentration of liquid-phase chemical warfare agents sprayed from the rooftop of the upwind building, while simultaneously increasing the influx into the urban street canyon, resulting in a higher concentration within the canyon. This indicates that incoming wind speed significantly affects the amount of chemical warfare agents entering the urban street canyon. As the dry deposition velocity increased, a significant decrease in concentration due to dry deposition was observed near the downwind building. While an increase in the evaporation rate of liquid-phase chemical warfare agents led to higher concentrations of gas agents, the diffusion range remained largely unchanged. The study confirmed that the dispersion and dry deposition of chemical warfare agents in urban street canyons are significantly influenced by the incoming wind speed and evaporation rate.

The dispersion model for non-reactive chemical warfare agents developed in this study has demonstrated the capability to simulate numerically the behavior and interaction of such agents within an urban

street canyon environment. Although this research focused on a simplified urban street canyon, actual urban areas are surrounded by numerous buildings and subject to a variety of meteorological conditions. Future work should aim to validate and improve the dispersion model in environments that consider more realistic meteorological conditions and building configurations, to enhance the accuracy of chemical warfare agent dispersion modeling in real-world scenarios.

References

Ahmad, A. L., Lau, K. K., & Bakar, M. A. (2005). Impact of different spacer filament geometries on concentration polarization control in narrow membrane channel. *Journal of Membrane Science*, 262(1-2), 138-152.

Ahmadi, M., Mirjalily, S. A. A., & Oloomi, S. A. A. (2020). Simulation of pollutant dispersion in urban street canyons using hybrid rans-les method with two-phase model. Computers & Fluids, 210, 104676.

Baek, D. H., & Yoon, Y. J. (2015). A Research for conducting successful Urban Operation in Korean peninsula. *Convergence Security Journal*, 15(3_1), 53-62.

Baik, J. J., Kang, Y. S., & Kim, J. J. (2007). Modeling reactive pollutant dispersion in an urban street canyon. Atmospheric Environment, 41(5), 934-949.

Becherini, F., Pastorelli, G., Valotto, G., Gambirasi, A., Bianchin, S., & Favaro, M. (2017). Effects of protective treatments on particle deposition and colour variation in stone surfaces exposed to an urban environment. *Progress in Organic Coatings*, 112, 75-85.

Bestion, D. (2012). Applicability of two-phase CFD to nuclear reactor thermal hydraulics and elaboration of Best Practice Guidelines. Nuclear Engineering and Design, 253, 311-321.

Chaudhary, M., & Singh, M. K. (2020). Study of multispecies convection-dispersion transport equation with variable parameters. *Journal of Hydrology*, 591, 125562.

Chen, G., Lam, C. K. C., Wang, K., Wang, B., Hang, J., Wang, Q., & Wang, X. (2021). Effects of urban geometry on thermal environment in 2D street canyons: A scaled experimental study. *Building and Environment*, 198, 107916.

Chew, L. W., & Norford, L. K. (2018). Pedestrian-level wind speed enhancement in urban street canyons with void decks. *Building and Environment*, 146, 64-76.

Cullis, I. G., Nikiforakis, N., Frankl, P., Blakely, P., Bennett, P., & Greenwood, P. (2016). Simulating geometrically complex blast scenarios. Defence technology, 12(2), 134-146.

Defense Threat Reduction Agency, "Hazard Prediction and Assessment Capability (HPAC) User's Guide", 2007.

Di Bernardino, A., Monti, P., Leuzzi, G., & Querzoli, G. (2018). Pollutant fluxes in two-dimensional street canyons. *Urban climate*, 24, 80-93.

FOLLOWS, H. (2005). Convention on the prohibition of the development, production, stockpiling and use of chemical weapons and on their destruction. Organization for the Prohibition of Chemical Weapons.

Giardina, M., & Buffa, P. (2018). A new approach for modeling dry deposition velocity of particles. *Atmospheric Environment*, 180, 11-22.

Gousseau, P., Blocken, B., & Van Heijst, G. J. F. (2011). CFD simulation of pollutant dispersion around isolated buildings: On the role of convective and turbulent mass fluxes in the prediction accuracy. *Journal of Hazardous Materials*, 194, 422-434.

Gromke, C., Buccolieri, R., Di Sabatino, S., & Ruck, B. (2008). Dispersion study in a street canyon with tree planting by means of wind tunnel and

numerical investigations–evaluation of CFD data with experimental data. *Atmospheric Environment*, 42(37), 8640–8650.

Hanna, S. R., Hansen, O. R., Ichard, M., & Strimaitis, D. (2009). CFD model simulation of dispersion from chlorine railcar releases in industrial and urban areas. *Atmospheric environment*, 43(2), 262–270.

Hayati, A. N., Stoll, R., Pardyjak, E. R., Harman, T., & Kim, J. J. (2019). Comparative metrics for computational approaches in non–uniform street–canyon flows. *Building and Environment*, 158, 16–27.

Hofman, J., Bartholomeus, H., Janssen, S., Calders, K., Wuyts, K., Van Wittenberghe, S., & Samson, R. (2016). Influence of tree crown characteristics on the local PM10 distribution inside an urban street canyon in Antwerp (Belgium): A model and experimental approach. *Urban forestry & urban greening*, 20, 265–276.

Hubbard, J. A., Haglund, J. S., & Ezekoye, O. A. (2009). Simulation of the evolution of particle size distributions containing coarse particulate in the atmospheric surface layer with a simple convection–diffusion–sedimentation model. *Atmospheric Environment*, 43(29), 4435–4443.

Jiang, H., Lu, L., & Sun, K. (2010). Simulation of particle deposition in ventilation duct with a particle–wall impact model. *Building and environment*, 45(5), 1184–1191.

Kang, G., & Kim, J. J. (2023). Effects of Vertical Forests on Air Quality in Step–up Street Canyons. *Sustainable Cities and Society*, 94, 104537.

Kim, J.–J., & Baik, J.–J. (2010). Effects of street–bottom and building–roof heating on flow in three–dimensional street canyons. *Advances in Atmospheric Sciences*, 27(3), 513–527.

Kukkonen, J., Riikonen, K., Nikmo, J., Jäppinen, A., & Nieminen, K. (2001). Modelling aerosol processes related to the atmospheric dispersion of sarin. *Journal of hazardous materials*, 85(3), 165-179.

Kwak, K. H., & Baik, J. J. (2014). Diurnal variation of NOx and ozone exchange between a street canyon and the overlying air. *Atmospheric Environment*, 86, 120-128.

Kwon, A-Rum, S. J., Park, G. Kang, J. J., Kim. (2020). Carbon Monoxide Dispersion in an urban area simulated by a CFD model coupled to the WRF-Chem model. *Korean Journal of Remote Sensing*, 36, 5-1.

Kye, Y. S., Chung, W. Y., Kim Y. J. (2008) A Study on the Chemical Warfare Agents dispersion modelling in a nautrally ventilated indoor system. Journal of the Korea Institute of Military Scinece and Technology, 11, 4

Law, W. P., Erain, N., Ramli, N. I., & Gimbun, J. (2019). Assessment of chlorine leak dispersion around Gebeng industrial area and potential evacuation route. *Atmospheric Research*, 216, 117-129.

Lee, J. M., Kang, Y. I., & Kim, J. H. (2014). A Study on the Field of View of the Remote FTIR Chemical Imaging Detection System. *Journal of the Korea Institute of Military Science and Technology*, 17(1), 122-128.

Lima, I. A., Parteli, E. J., Shao, Y., Andrade, J. S., Herrmann, H. J., & Araújo, A. D. (2020). CFD simulation of the wind field over a terrain with sand fences: Critical spacing for the wind shear velocity. Aeolian Research, 43, 100574.

Linda, J., Pospíšil, J., & Köbölová, K. (2022). Identification of Wind-Induced Particle Resuspension in Urban Environment Using CFD Modelling. Atmosphere, 14(1), 57.

Lu, K. F., & Peng, Z. R. (2023). Impacts of viaduct and geometry configurations on the distribution of traffic-related particulate matter in urban street canyon. *Science of The Total Environment*, 858, 159902.

Miao, C., Yu, S., Hu, Y., Liu, M., Yao, J., Zhang, Y., ... & Chen, W. (2021). Seasonal effects of street trees on particulate matter concentration in an urban street canyon. *Sustainable Cities and Society*, 73, 103095.

Montoya, M. I., Planas, E., & Casal, J. (2009). A comparative analysis of mathematical models for relating indoor and outdoor toxic gas concentrations in accidental releases. *Journal of Loss Prevention in the Process Industries*, 22(4), 381-391.

Mukhopadhyay, S., Schoenitz, M., & Dreizin, E. L. (2021). Vapor-phase decomposition of dimethyl methylphosphonate (DMMP), a sarin surrogate, in presence of metal oxides. Defence Technology, 17(4), 1095-1114.

Park, S. J., Kim, J. J., Choi, W., Kim, E. R., Song, C. K., & Pardyjak, E. R. (2020). Flow characteristics around step-up street canyons with various building aspect ratios. *Boundary-Layer Meteorology*, 174, 411-431.

Park, S. J., Kim, J. J., Kim, M. J., Park, R. J., & Cheong, H. B. (2015). Characteristics of flow and reactive pollutant dispersion in urban street canyons. *Atmospheric Environment*, 108, 20-31.

Pontiggia, M., Derudi, M., Alba, M., Scaioni, M., & Rota, R. (2010). Hazardous gas releases in urban areas: Assessment of consequences through CFD modelling. Journal of hazardous materials, 176(1-3), 589-596.

Pontiggia, M., Derudi, M., Busini, V., & Rota, R. (2009). Hazardous gas dispersion: a CFD model accounting for atmospheric stability classes. *Journal of hazardous materials*, 171(1-3), 739-747.

Pugh, T. A., MacKenzie, A. R., Whyatt, J. D., & Hewitt, C. N. (2012). Effectiveness of green infrastructure for improvement of air quality in urban street canyons. *Environmental science & technology*, 46(14), 7692-7699.

Sanchez, B., Santiago, J. L., Martilli, A., Palacios, M., & Kirchner, F. (2016). CFD modeling of reactive pollutant dispersion in simplified urban configurations with different chemical mechanisms. *Atmospheric Chemistry and Physics*, *16*(18), 12143-12157.

Song, J. Y., & Yoon, S. W. (2012). Analysis on the Risk of Explosive Terror in Domestic Buildings. *Journal of Korean Association for Spatial Structures*, 12(2), 73-80.

Takano, Y., & Moonen, P. (2013). On the influence of roof shape on flow and dispersion in an urban street canyon. *Journal of Wind Engineering and Industrial Aerodynamics*, 123, 107-120.

Tan, W., Li, C., Wang, K., Zhu, G., & Liu, L. (2019). Geometric effect of buildings on the dispersion of carbon dioxide cloud in idealized urban street canyons. Process Safety and Environmental Protection, 122, 271-280.

Tominaga, Y., & Stathopoulos, T. (2011). CFD modeling of pollution dispersion in a street canyon: Comparison between LES and RANS. Journal of Wind Engineering and Industrial Aerodynamics, 99(4), 340-348.

Tominaga, Y., & Stathopoulos, T. (2012). CFD modeling of pollution dispersion in building array: evaluation of turbulent scalar flux modeling in RANS model using LES results. *Journal of Wind Engineering and Industrial Aerodynamics*, 104, 484-491.

Tominaga, Y., Okaze, T., & Mochida, A. (2018). Wind tunnel experiment and CFD analysis of sand erosion/deposition due to wind around an obstacle. Journal of Wind Engineering and Industrial Aerodynamics, 182, 262-271.

Vardoulakis, S., Fisher, B. E., Pericleous, K., & Gonzalez-Flesca, N. (2003). Modelling air quality in street canyons: a review. *Atmospheric environment*, 37(2), 155-182.

Vogel, J. M., Lucheta, R., Zinn, B., & Trigg, J. (2022). Development of fire model source terms and effects in the Hazard Prediction and Assessment Capability (HPAC) atmospheric transport and dispersion code. Atmospheric Environment: X, 14, 100166.

Wang, B., Cot, L. D., Adolphe, L., Geoffroy, S., & Sun, S. (2017). Cross indicator analysis between wind energy potential and urban morphology. *Renewable Energy*, 113, 989-1006.

Wang, J. W., & Kim, J. J. (2015). A study on sensitivity of pollutant dispersion to inflow wind speed and turbulent Schmidt number in a street canyon. *Atmosphere*, 25(4), 659-667.

Willis, M. P., Mantooth, B. A., & Lalain, T. A. (2012). Novel methodology for the estimation of chemical warfare agent mass transport dynamics. Part II: absorption. The Journal of Physical Chemistry C, 116(1), 546-554.

Xiang, L., Meng, Q., & Ren, P. (2023). Effects of environmental and architectural factors on chloride-salt deposition on coastal building surfaces in the Zhujiang River Estuary. *Building and Environment*, 110554.

Yakhot, V. S. A. S. T. B. C. G., Orszag, S. A., Thangam, S., Gatski, T. B., & Speziale, C. (1992). Development of turbulence models for shear flows by a double expansion technique. *Physics of Fluids A: Fluid Dynamics*, 4(7), 1510-1520.

Yakhot, V., & Smith, L. M. (1992). The renormalization group, the ε-expansion and derivation of turbulence models. *Journal of scientific computing*, 7, 35-61.

Yanagisawa, N., Morita, H., & Nakajima, T. (2006). Sarin experiences in Japan: acute toxicity and long-term effects. Journal of the neurological sciences, 249(1), 76-85.

Yang, H. J., & Kim, J. J. (2015). Assessment of observation environment for surface wind in urban areas using a CFD model. *Atmosphere*, 25(3), 449-459.

Zhang, L., Gong, S., Padro, J., & Barrie, L. (2001). A size-segregated particle dry deposition scheme for an atmospheric aerosol module. *Atmospheric environment*, 35(3), 549-560.

Zhang, Z., & Chen, Q. (2009). Prediction of particle deposition onto indoor surfaces by CFD with a modified Lagrangian method. *Atmospheric Environment*, 43(2), 319-328.

Zhao, B., & Wu, J. (2009). Effect of particle spatial distribution on particle deposition in ventilation rooms. *Journal of hazardous materials*, 170(1), 449-456.

Appendix

The dry deposition velocity (V_d) is represented as follows.

$$V_d = V_g + \frac{1}{(R_a + R_s)} \quad (1)$$

where, V_g is settling velocity, R_a is aerodynamic resistance, R_s is surface resistance. The gravitational settling is calculated as

$$V_g = \frac{\rho {d_p}^2 g C}{18\nu} \quad (2)$$

where, ρ denotes the particle density, d_p is the particle diameter, g represents the gravity acceleration, and ν is the viscosity coefficient of air. The correction factor for small particles (C) is expressed as follows:

$$C = 1 + \frac{2\lambda}{d_p}\left(1.257 + 0.4e^{-\frac{0.55 d_p}{\lambda}}\right) \quad (3)$$

where, λ is the mean free path of air molecules depending on temperature, pressure, and kinematics viscosity of air. The aerodynamic resistance is calculated as follows:

$$R_a = \frac{\ln\left(\frac{z_R}{z_0}\right) - \psi_H}{\kappa u_*} \quad (4)$$

where, z_R is the altitude at which V_d is calculated. ψ_H is the stability

function. In this study, since urban areas are the focus of the numerical experiments, the constant values for urban areas as suggested by Zhang et al. (2008) were utilized. The R_s, which depends on the size of the depositing particles, atmospheric conditions, and surface characteristics of the terrain, is as follows:

$$R_s = \frac{1}{\varepsilon_0 u_* (E_B + E_{IM} + E_{IN}) R_1} \quad (5)$$

where, E_B denotes Brownian diffusion, E_{IM} represents impaction, E_{IN} is used for calculating collection efficiency by interception. R_1 is the correction factor representing the fraction of particles.

Acknowledgements

This work was funded by the Agency for Defense Development (Grant No. UI230006TD).